



# COST1 regulates autophagy to control plant drought tolerance

Yan Bao<sup>a,b,c,1,2</sup> , Wei-Meng Song<sup>b,d,1</sup>, Peipei Wang<sup>e</sup>, Xiang Yu<sup>b</sup>, Bei Li<sup>d</sup>, Chunmei Jiang<sup>d</sup>, Shin-Han Shiu<sup>e,f</sup> , Hongxia Zhang<sup>b,d,g,2</sup>, and Diane C. Bassham<sup>a,2</sup>

<sup>d</sup>College of Agriculture, Ludong University, 264025 Yantai, China; <sup>a</sup>Department of Genetics, Development and Cell Biology, Iowa State University, Ames, IA 50011; <sup>b</sup>National Key Laboratory of Plant Molecular Genetics, Shanghai Institute of Plant Physiology and Ecology, Chinese Academy of Sciences, 200032 Shanghai, China; <sup>c</sup>Department of Biochemistry and Molecular Biology, Michigan State University, East Lansing, MI 48824; <sup>e</sup>Department of Plant Biology, Michigan State University, East Lansing, MI 48824; <sup>f</sup>Department of Computational Mathematics, Science, and Engineering, Michigan State University, East Lansing, MI 48824; and <sup>g</sup>Key Laboratory of Molecular Module-Based Breeding of High Yield and Abiotic Resistant Plants in Universities of Shandong, Ludong University, 264025 Yantai, Shandong Province, China

Edited by Richard D. Vierstra, Washington University in St. Louis, St. Louis, MO, and approved February 19, 2020 (received for review October 23, 2019)

**Plants balance their competing requirements for growth and stress tolerance via a sophisticated regulatory circuitry that controls responses to the external environments. We have identified a plant-specific gene, *COST1* (constitutively stressed 1), that is required for normal plant growth but negatively regulates drought resistance by influencing the autophagy pathway. An *Arabidopsis thaliana cost1* mutant has decreased growth and increased drought tolerance, together with constitutive autophagy and increased expression of drought-response genes, while overexpression of *COST1* confers drought hypersensitivity and reduced autophagy. The *COST1* protein is degraded upon plant dehydration, and this degradation is reduced upon treatment with inhibitors of the 26S proteasome or autophagy pathways. The drought resistance of a *cost1* mutant is dependent on an active autophagy pathway, but independent of other known drought signaling pathways, indicating that *COST1* acts through regulation of autophagy. In addition, *COST1* colocalizes to autophagosomes with the autophagosome marker ATG8e and the autophagy adaptor NBR1, and affects the level of ATG8e protein through physical interaction with ATG8e, indicating a pivotal role in direct regulation of autophagy. We propose a model in which *COST1* represses autophagy under optimal conditions, thus allowing plant growth. Under drought, *COST1* is degraded, enabling activation of autophagy and suppression of growth to enhance drought tolerance. Our research places *COST1* as an important regulator controlling the balance between growth and stress responses via the direct regulation of autophagy.**

resistant 1) is a positive regulator of drought responses that acts downstream of H<sub>2</sub>O<sub>2</sub> signaling (18). Genetic studies indicate an interplay between ABA and H<sub>2</sub>O<sub>2</sub>, suggesting that ABI1 acts upstream of H<sub>2</sub>O<sub>2</sub> while ABI2 is downstream (19).

The 26S proteasome-mediated protein turnover plays a critical role in plant stress responses, including those to drought (5, 20). During stress conditions, targeted proteins are specifically recognized and ubiquitinated via a sequential relay of an E1 activation enzyme, E2 conjugation enzyme, and an E3 ligase (21). Poly-ubiquitinated proteins are then subjected to degradation by the 26S proteasome, providing a mechanism for precise regulation of signaling (21). Protein turnover during various environmental stresses can also be mediated by autophagy (22, 23). Upon the induction of autophagy, a double-membrane structure engulfs unwanted cellular components, including individual proteins, protein aggregates, and organelles, forming an autophagosome, and transports them to the central vacuole for degradation and recycling (24). A number of genes, termed *ATG* (autophagy-related) genes, have been identified as required for autophagosome

autophagy | drought | *Arabidopsis* | *COST1*

**D**rought is an increasing problem worldwide because of water shortage and climate change, and is responsible for substantial yield loss in crops (1, 2). Plants have evolved sophisticated mechanisms for sensing and responding to drought, which involve perception of the stress, signal transduction, and physiological adaptations (3–5). Major signaling pathways have been identified for plant responses to drought, including those triggered by the drought-inducible phytohormone abscisic acid (ABA) (3) and the reactive oxygen species H<sub>2</sub>O<sub>2</sub>. Drought stimulates the biosynthesis of ABA (6, 7), which is subsequently bound by its receptor PYR/PRL/RCAR, leading to activation of the SnRK2 (SNF1-related kinases subfamily 2) family protein kinases (8–11). Active SnRK2 kinase then phosphorylates SLAC1 (S-type anion channel) and KAT1 (potassium channel), thus modulating stomatal movement (12–14).

Two plasma membrane NADPH (nicotinamide adenine dinucleotide phosphate, reduced form) oxidases, respiratory burst oxidase homologs D and F (RbohD/F), are responsible for the production of H<sub>2</sub>O<sub>2</sub> (15), which can activate Ca<sup>2+</sup> channels to favor stomatal closure (16). RbohF is phosphorylated by OST1 (open stomata 1) to favor H<sub>2</sub>O<sub>2</sub> production (17). A receptor-like kinase family protein GHR1 (guard cell hydrogen peroxide-

## Significance

**Drought is one of the most devastating threats to agricultural sustainability worldwide. Autophagy is known to be critical for plant responses to multiple stresses, including drought, but a direct link between drought tolerance and autophagy is still lacking. We report here the identification of a plant-specific protein, *COST1* (constitutively stressed 1), which attenuates autophagy under optimal growth conditions, thus controlling the trade-off between plant growth and stress tolerance. In addition to expanding our understanding of the regulation of autophagy in plants, the enhanced drought tolerance of a *cost1* mutant and the high conservation of *COST* proteins throughout the plant kingdom also indicates a potential for engineering *COST1* to enhance stress tolerance in crops.**

Author contributions: Y.B., H.Z., and D.C.B. designed research; Y.B. led the project; Y.B., W.-M.S., and P.W. performed research; P.W., X.Y., B.L., and C.J. contributed new reagents/analytic tools; Y.B., S.-H.S., and D.C.B. analyzed data; and Y.B., S.-H.S., and D.C.B. wrote the paper.

The authors declare no competing interest.

This article is a PNAS Direct Submission.

Published under the PNAS license.

Data deposition: RNA-seq analysis were deposited in the National Center for Biotechnology Information Gene Expression Omnibus (GEO) database, <https://www.ncbi.nlm.nih.gov/geo> (accession no. GSE113515).

<sup>1</sup>Y.B. and W.-M.S. contributed equally to this work.

<sup>2</sup>To whom correspondence may be addressed. Email: baoyan@msu.edu, hxzhang@sibs.ac.cn, or bassham@iastate.edu.

This article contains supporting information online at <https://www.pnas.org/lookup/suppl/doi:10.1073/pnas.1918539117/-DCSupplemental>.

First published March 13, 2020.

formation or delivery to the vacuole (25, 26). In addition, specific cargo can be selected for autophagy by cargo receptors, such as NBR1 (neighbor of BRCA1), which recognizes protein aggregates (27–29). Autophagy has a pivotal role in plant responses to a broad array of biotic and abiotic stresses, including drought, salt, oxidative stress, flooding, and pathogens (30–34).

In this study, we identified a plant-specific DUF641 family protein that we named COST1 (constitutively stressed 1). A *cost1* mutant has defects in development, a strong drought-resistance phenotype, and constitutive activation of autophagy. Consistently, overexpression of *COST1* leads to drought hypersensitivity and decreased autophagy in response to stress. The drought tolerance of the *cost1* mutant requires an intact autophagy pathway and COST1 interacts directly with ATG8e, a key factor required for autophagy. We propose a model in which COST1 negatively regulates autophagy, and aggregation/degradation of COST1 during drought therefore activates autophagy, allowing plants to tolerate drought conditions.

## Results

**A *cost1* Mutant Has Pleiotropic Growth Defects.** To date, in the genome of *Arabidopsis thaliana*, over 40% of all protein-encoding genes are classified as having unknown function or are poorly characterized (35), despite many efforts to identify gene functions (36, 37). Here, we identified a plant-specific protein (AT2G45260) containing a DUF641 (domain of unknown function 641) domain. We named this gene *COST1*, based on the stress-tolerant phenotype of a *cost1* knockout mutant we later observed (see below). BLAST search against TAIR10 (The Arabidopsis Information Resource, [arabidopsis.org](http://arabidopsis.org)) and alignment analysis indicated that 13 COST-related proteins are present in *A. thaliana* and share sequence similarity at their N termini, which contains the DUF641 domain (Fig. 1A and *SI Appendix, Fig. S1*). Based on precomputed results from Pfam (38) and sequence analysis (*Materials and Methods*), DUF641 family proteins (referred to as COST proteins) are plant-specific and can be found widely throughout land plants, including mosses, but are absent from algae (Fig. 1B and *SI Appendix, Fig. S2*). COST proteins can be classified into six subfamilies, and the duplication between the subfamily containing COST1 and subfamily Branch\_1 happened before the divergence of seed plants (Fig. 1B and *SI Appendix, Figs. S1 and S2*).

Eight of the 12 angiosperm species examined in our study have only one copy of the *COST1* gene. Due to the repeated polyploidization events in flowering plants, the majority of genes have  $\geq 1$  duplicate (39). In addition, genes with housekeeping functions that are subject to strong selective pressure tend to be maintained as single copies across species (40). Thus, the conserved phylogenetic distribution of the low copy number of *COST1* suggests that it is subject to strong selection to retain one copy. In four species with *COST1* duplicates, three (*Brassica rapa*, *Populus trichocarpa*, and *Zea mays*) have relatively recent whole-genome duplication events (41). *A. thaliana* has three closely related *COST1*-like genes (*COST2* to *-4*) that were derived from duplication events after the divergence between *A. thaliana* and *Arabidopsis lyrata* lineages (Fig. 1B). *COST2* and *-4* are both truncated at the latter halves of the genes compared to *COST1*. *COST3*, on the other hand, shares similarity over its entire length of *COST1* but has a premature stop codon. Together with our findings that the transcripts of *COST2/4* and *COST3* are undetectable or at an extremely low level, respectively, by RNA sequencing (RNA-seq) and qPCR when compared with *COST1* (Fig. 1B and C), these findings suggest that *COST2* to *-4* may be pseudogenes.

To characterize the function of *COST1* in *Arabidopsis*, a T-DNA insertion line, SALK\_064001, was obtained from the *Arabidopsis* Biological Resource Center. Genomic PCR showed that the insertion in *cost1* is homozygous, and qPCR indicated complete loss of transcript in the mutant background (*SI*

*Appendix, Fig. S3 A–C*). The *cost1* mutation dramatically affected plant growth; compared with WT (wild-type, Columbia-0) plants, *cost1* has smaller leaves and reduced plant height (Fig. 1D and *SI Appendix, Fig. S3 D and E*). Microscopy analysis of the leaves indicated that the reduced plant size is caused by reduced cell size (*SI Appendix, Fig. S3 F and G*). The mutant also has dark green leaves that could be attributed to increased chlorophyll per equivalent fresh weight (*SI Appendix, Fig. S3H*).

***cost1* Mutant Has Increased Drought Tolerance.** Based on the observation of the small, dark green phenotype of the *cost1* mutant, we hypothesized that *cost1* may be stressed and function in ABA or stress responses. We first tested the drought response of *cost1* by withholding water for 2 wk and found that the *cost1* mutant is more resistant to drought than WT plants (Fig. 2A and *SI Appendix, Fig. S4A*). To confirm that the *cost1* phenotype is caused by disruption of the *COST1* gene, the *COST1* genomic sequence including 670 bp upstream of the start codon, the full-length *COST1* coding sequence, and 540 bp downstream was introduced into the *cost1* mutant background by *Agrobacterium*-mediated floral dip (42). The complementation lines generated expressed the *COST1* gene, and were identical to WT in growth, drought tolerance, and water loss assays (*SI Appendix, Fig. S4*).

To further demonstrate that the mutant phenotype is correlated with the *COST1* expression level, we generated RNAi-*COST1* lines with reduced *COST1* expression (*SI Appendix, Fig. S5A*). RNAi-*COST1* lines showed drought resistance and lower water loss than WT, similar to the phenotype observed in the *cost1* mutant (Fig. 2B and C). In addition, the RNAi lines and *cost1* mutant had a smaller stomatal aperture and higher proline content than WT (*SI Appendix, Fig. S5 B–D*), which further indicates that COST1 is a negative regulator of drought responses. The expression patterns of nine dehydration-induced genes—*RD29A*, *ABI2*, *ABI5*, *PP2C*, *RD22*, *COR15A*, *KIN1*, *COR414-TM1*, and *LTP3* (43, 44)—were tested by qPCR in WT and *cost1* plants with or without dehydration treatment. As constitutively higher expression of these genes was observed in unstressed *cost1*, when compared with WT, with even higher expression in dehydrated *cost1* plants, this supports a role for COST1 in drought responses (Fig. 2D).

**Disruption of *COST1* Causes Broad Induction of Stress-Responsive Genes.** To reveal the underlying mechanism of COST1 function in the drought response, we examined the transcriptome of 10-d-old WT and *cost1* plants under control and dehydration conditions by RNA-seq (Fig. 2E). Statistically differentially expressed genes (DEGs; fold-change > 2) were evaluated and a gene ontology (GO) enrichment analysis supported the role of *COST1* in drought tolerance, as many stress-associated pathways were significantly enriched in the gene set (Fig. 2F–H). Among these drought up-regulated genes, 52 genes were constitutively induced in the *cost1* mutant background when compared with WT (Fig. 2F). Importantly, 86 genes were constitutively up-regulated and 20 genes were constitutively down-regulated in the *cost1* mutant, even without dehydration treatment (Fig. 2F and G). The up-regulated gene set is highly enriched in water deprivation, ABA, salt, and cold pathway functions, while there is significant enrichment in photosynthesis-related pathways in the down-regulated genes (Fig. 2H and I). This transcriptome analysis was consistent with the phenotype (increased drought tolerance and reduced plant growth) we observed in *cost1* (Fig. 2A and B), indicating an important role for COST1 in drought responses.

**Drought-Mediated *COST1* Protein Relocation and Its Degradation through the 26S-Proteasome and Autophagy.** Many stress-related genes are transcriptionally regulated (45). To test the effect of different stresses on *COST1* transcript levels, 10-d-old WT seedlings were treated with NaCl, ABA, mannitol, or drought and the

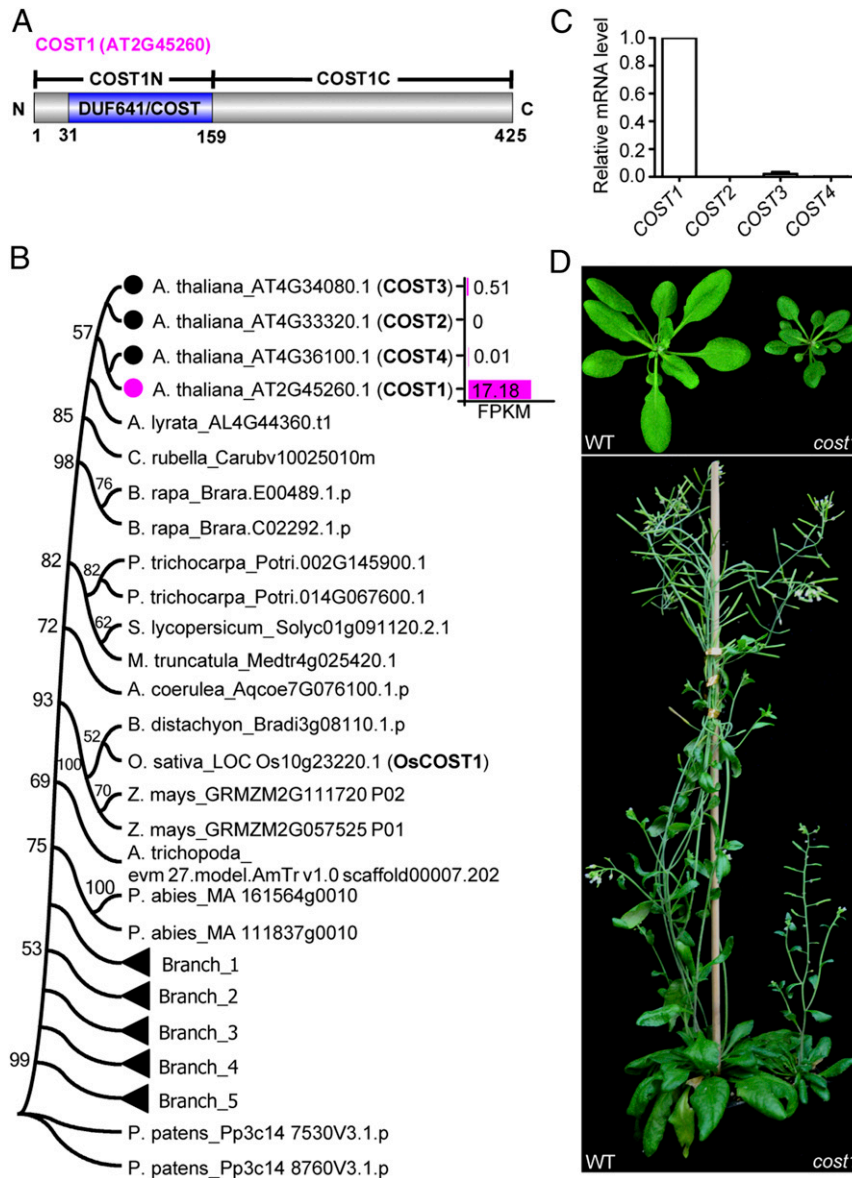


**Fig. 1.** A conserved plant-specific COST1 (ID: AT2G45260) protein required for normal growth and development. (A) Schematic diagram of the structure of the COST1 protein; the conserved DUF641 domain is indicated at the N terminus (N); numbers below indicate the position of amino acids. (B) Phylogenetic analysis of COST proteins in different plant species. The numbers on the branch node refer to bootstrap value of the phylogenetic tree; 500 bootstrap replicates were performed. Dots denote the four *Arabidopsis* COST proteins, with COST1 shown in magenta. Fragments per kilobase of transcript per million mapped reads (FPKM) values of the four *Arabidopsis* COST genes are shown on the right based on the RNA-seq in this study. Protein IDs are listed after abbreviated species names. The full species names are (from top to bottom): *Arabidopsis thaliana*, *Arabidopsis lyrata*, *Capsella rubella*, *Brassica rapa*, *Populus trichocarpa*, *Solanum lycopersicum*, *Medicago truncatula*, *Aquilegia coerulea*, *Brachypodium distachyon*, *Oryza Sativa*, *Zea mays*, *Amborella trichopoda*, *Picea abies*, and *Physcomitrella patens*. Triangles represent hidden subtrees, which are shown in detail in *SI Appendix, Fig. S2*. (C) Analysis of expression of the *Arabidopsis* COST genes by qPCR. (D) Pleiotropic defects of a *cost1* mutant. Four-week-old and 45-d-old WT and *cost1* plants are shown in the *Upper* and *Lower*, respectively.

expression of *COST1* was assessed by qPCR. Unexpectedly, no significant difference was found under any stress tested when compared with control conditions (*SI Appendix, Fig. S6A*). In addition, transgenic *Arabidopsis* lines were generated expressing GUS driven by the *COST1* promoter. Ten-day-old transgenic seedlings harboring ProCOST1-GUS were stained for GUS activity, confirming that *COST1* expression does not change significantly in response to drought (*SI Appendix, Fig. S6B*).

We then hypothesized that drought could potentially affect the stability of the COST1 protein, instead of its transcript level. To test this hypothesis, transgenic plants expressing COST1-YFP under a constitutive CaMV 35S promoter in the *cost1* mutant background were generated. While under control conditions

the YFP signal appeared throughout the cytoplasm, fluorescent puncta were observed when COST1-YFP transgenic plants were subjected to dehydration (Fig. 3 *A* and *B*), indicating a change in localization. There was also a significant reduction in the fluorescence intensity of COST1-YFP after dehydration when compared with control samples (Fig. 3 *A* and *C*). In addition, COST1-YFP protein degradation was observed over a time course of dehydration treatment; immunoblotting analysis detected an ~30% decrease in COST1-YFP when treated for 6 h (Fig. 3*D*).

The primary general mechanisms for protein degradation in plant cells are via the 26S proteasome pathway (46) or by vacuole-mediated bulk protein degradation, generally through the autophagy

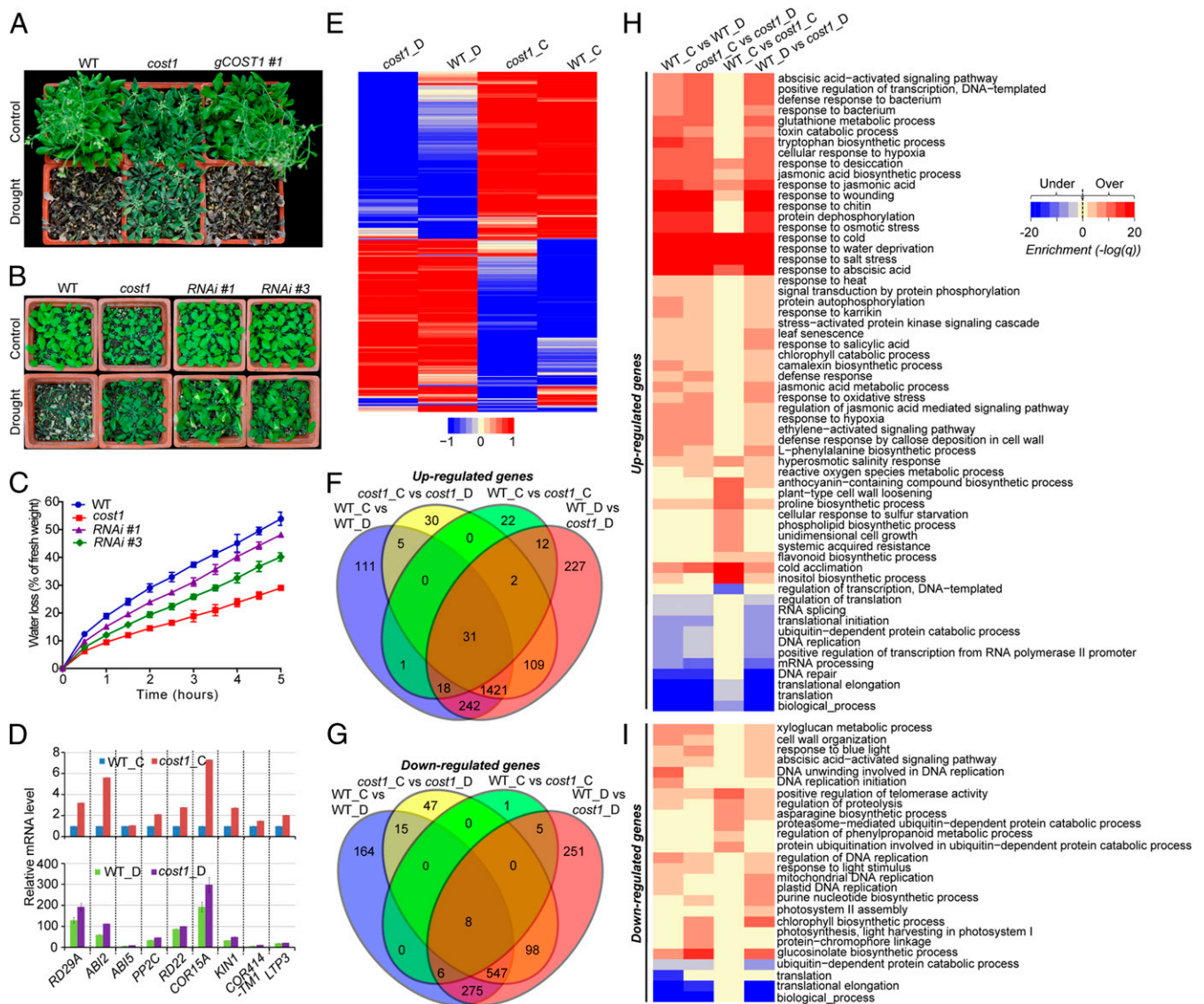


**Fig. 2.** Knockout of *COST1* confers drought tolerance and induces the expression of a spectrum of stress-responsive genes. (A and B) WT, *cost1* (*cost1-1*), *gCOST1*#1 (complementation line with *COST1* genomic DNA), and two *COST1* RNAi lines (*COST1*-RNAi#1 and *COST1*-RNAi#3) were subjected to drought treatment for 2 wk, and the water loss of detached rosette leaves from each genotype was recorded every 30 min for 5 h (C). (D) Expression of representative drought responsive genes in WT and *cost1* with and without drought treatment was assessed by qPCR. (E) Clustering of DEGs (fold-change in expression level >2 between two samples) in WT and *cost1* plants with and without dehydration treatment, “C” denotes control and “D” denotes dehydration. Color legend denotes normalized gene-expression value. (F and G) Comparison of drought-regulated DEGs in whole-transcriptome RNA-seq. (H and I) Enrichment of Biological Process GOs in drought-regulated DEGs. Color scale:  $-\log_{10}$  (adjusted *P* value). Over- and underrepresentation are shown in red and blue, respectively.

pathway (25). To assess whether the 26S proteasome or autophagy are required for *COST1* degradation, *COST1*-YFP seedlings (*cost1-1* mutant background, with full complementation) were incubated with the proteasome inhibitor MG132 or the vacuolar degradation inhibitor ConcanamycinA (ConcA) over a time course of dehydration treatment. *COST1*-YFP protein accumulated after the dehydration treatment upon MG132 or ConcA incubation, compared with the DMSO (dimethylsulfoxide) control (Fig. 3 E and F). Immunoprecipitation using GFP-Trap demonstrated that *COST1*-YFP was ubiquitinated, with more *COST1*-YFP ubiquitination detected upon dehydration compared with the control (Fig. 3G and SI Appendix, Fig. S7). These results indicate that dehydration can induce the ubiquitination of *COST1*, which is then subjected to degradation by both the 26S proteasome and autophagy.

**Colocalization of *COST1* with *ATG8* and *NBR1*.** To provide insight into the potential function of *COST1*, we assessed in more detail its subcellular localization. Upon transient expression of *COST1*-YFP in *Arabidopsis* protoplasts, punctate structures were observed. However, no colocalization was seen when we coexpressed *COST1*-YFP with organelle markers, including peroxisome (mCherry-peroxisome), Golgi (mCherry-Golgi), and PVC markers (mRFP-VSR2 and mCherry-Rha1) (47, 48) (SI Appendix, Fig. S8). Interestingly, constantly moving dots are observed in *COST1*-YFP transgenic plants upon dehydration treatment (Movie S1); we hypothesized that these dots may be autophagosomes, given the critical role of autophagy in the drought response (30, 31).

To test this hypothesis, we cotransformed protoplasts with *COST1*-YFP and mCherry-ATG8e, a marker that labels both autophagosomes in the cytoplasm and autophagic bodies after

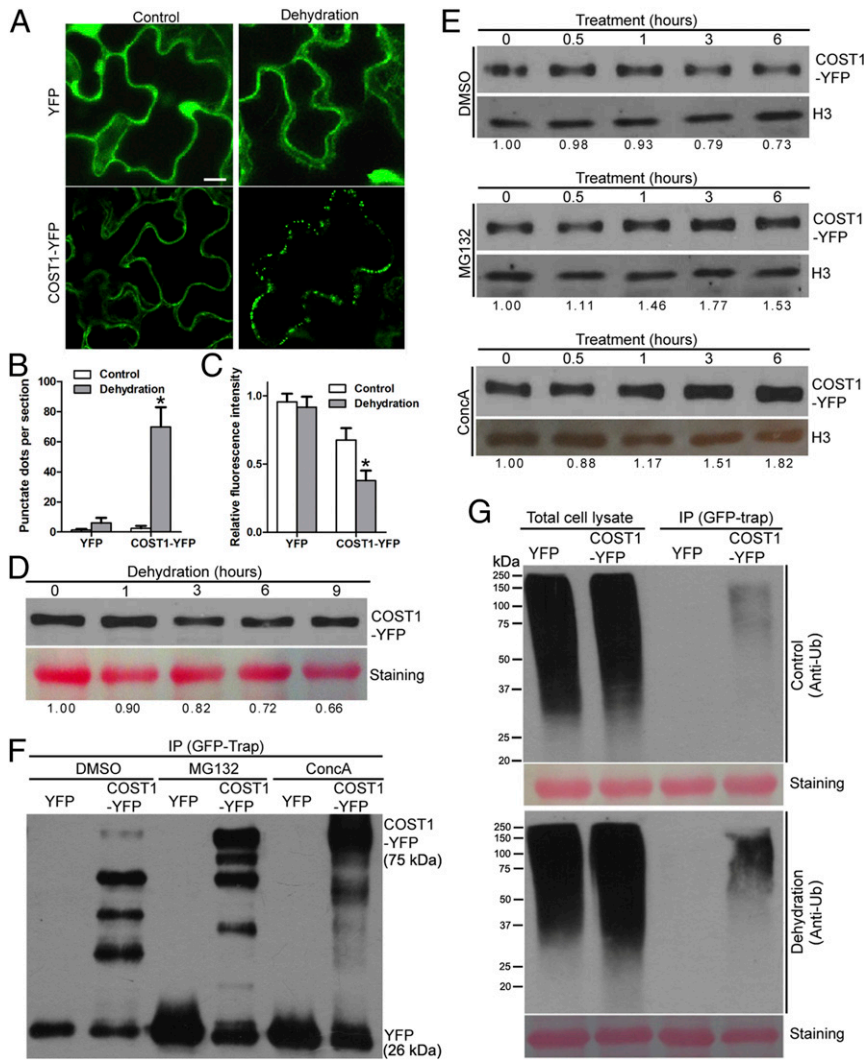


**Fig. 3.** Expression of COST1 during drought stress. (A) Localization and characteristics of COST1-YFP protein after 3 h of dehydration treatment. (Scale bar, 10  $\mu$ m.) (B and C) Quantification of fluorescence intensity and punctate structures before and after 3 h of dehydration treatment. Signals were quantified for at least 10 images per replicate, with 3 biological replicates. Asterisks indicate significant differences, compared with no treatment. (D) Immunoblot of COST1-YFP protein after dehydration treatment for the indicated times using antibodies against GFP. The number below indicates the band intensity of COST1-YFP, and Ponceau staining was used as a loading control. (E) Immunoblot of COST1-YFP protein after treatment with DMSO (control), MG132, or ConcA. (F) COST1-YFP was immunoprecipitated after treatment with DMSO, MG132, or ConcA under normal conditions, followed by detection using anti-GFP antibodies. (G) Ubiquitination of COST1-YFP after dehydration of 10-d-old COST1-YFP or YFP transgenic plants for 6 h. After immunoprecipitation with GFP-trap, samples were immunoblotted using antibodies against ubiquitin. Transgenic COST1-YFP plants were generated in *cost1* mutant background with full complementation.

delivery to the vacuole. We found that the two proteins colocalized (Fig. 4 A, Upper), suggesting that COST1-YFP is found in autophagosomes or autophagic bodies. In plants, the selective autophagy adaptor NBR1 has been reported to interact and colocalize with ATG8 (28, 49). NBR1 specifically binds to ubiquitinated proteins and recruits them to autophagosomes for degradation (23, 27). COST1-YFP also colocalized with mCherry-NBR1 puncta (Fig. 4 A, Lower), which are likely to correspond both to autophagosomes and to ubiquitinated protein aggregates.

**Direct Interaction of COST1 with ATG8e.** We assessed whether COST1 and ATG8 can directly interact using a split luciferase assay in tobacco leaves (Fig. 4B) (50). cLUC-ATG8e interacted with COST1-nLUC, while the negative controls cLUC plus nLUC, cLUC-ATG8e plus GFP-nLUC, and cLUC-GFP plus COST1-nLUC did not interact. Next, we performed pull-down assays to confirm this interaction using GST or a GST-COST1 fusion as bait to precipitate His-ATG8e protein (SI Appendix, Fig. S9). As shown

in Fig. 4C, GST-COST1 protein bound specifically to His-ATG8e but GST alone did not. Finally, coimmunoprecipitation (co-IP) analysis after transient expression in tobacco leaves also showed that COST1-Flag could specifically precipitate GFP-ATG8e but not the GFP protein alone (Fig. 4D).

**Drought Tolerance of *cost1* Is Dependent on Autophagy.** As *COST1* is a previously uncharacterized gene involved in drought tolerance, we determined its genetic relationship to existing drought signaling pathways. ABA and H<sub>2</sub>O<sub>2</sub>-dependent signaling pathways play a major role in regulating drought responses. To test whether COST1 functions in ABA signaling, *cost1* was crossed with *abi1-1C*, a gain-of-function mutant in the ABA signaling pathway (51, 52); with *ost1*, an SnRK2 protein kinase-null mutant in ABA and H<sub>2</sub>O<sub>2</sub> signal transduction (53); and with *aba3*, an ABA biosynthesis-deficient mutant (54). To test the relationship of *cost1* to H<sub>2</sub>O<sub>2</sub> signaling, *cost1* was crossed with *ghr1* (18), another H<sub>2</sub>O<sub>2</sub> signaling-deficient mutant. As shown in SI Appendix, Fig. S10 A–D,

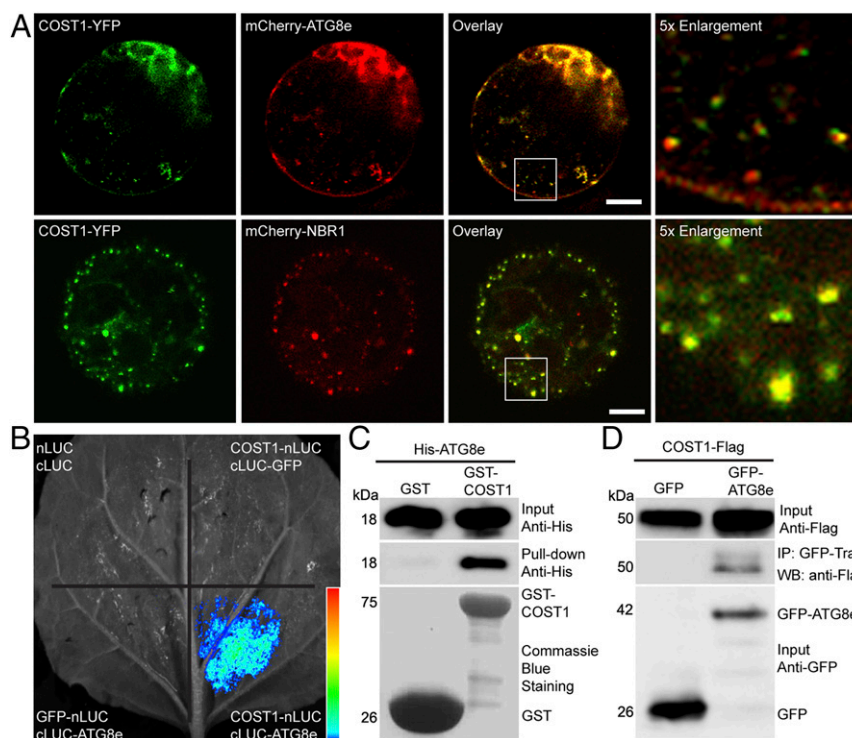


**Fig. 4.** Direct interaction between COST1 and ATG8e. (A) Colocalization of COST1-YFP with mCherry-ATG8e and mCherry-NBR1. (Scale bar, 10  $\mu\text{m}$ .) (B) Split luciferase analysis of the interaction between COST1-nLUC and cLUC-GFP. Different combinations of GFP-nLUC and cLUC-GFP with and without COST1 or ATG8e were used as negative controls. (C) GST pull-down assay between GST-COST1 and His-ATG8e. GST alone was used as negative control. (D) Co-IP of COST1-Flag with GFP-ATG8e. *Agrobacterium*-mediated coinfiltrations were carried out in tobacco leaves with combinations of 35S:GFP and 35S:COST1-Flag, and 35S:GFP-ATG8e and 35S:COST1-Flag. After 2 d of incubation, leaves were ground in liquid nitrogen and proteins immunoprecipitated with GFP-Trap. The immunoblot was probed with anti-GFP and anti-Flag antibodies. Leaves expressing 35S:GFP alone were used as a negative control.

in a water loss assay, each of the double mutants had phenotypes intermediate between the corresponding single mutants; this suggests that COST1 acts independently of ABA and  $\text{H}_2\text{O}_2$  signaling pathways. In addition, no significant difference from WT was observed in seed germination when *cost1* mutant seeds were germinated on half MS (Murashige and Skoog) media supplemented with ABA (*SI Appendix*, Fig. S11), also suggesting that COST1 functions independently of ABA signaling.

Autophagy is required for drought tolerance in *Arabidopsis*, and autophagy-deficient mutants are hypersensitive to drought (30). In addition, COST1 colocalizes with autophagosome markers and directly interacts with ATG8e (Fig. 4), indicating a potential relationship to autophagy. To test the relationship between *cost1* and the autophagy pathway, *cost1* was crossed with *atg5-1* and *atg7-2* as representative autophagy-deficient mutants (55, 56). In contrast to ABA and  $\text{H}_2\text{O}_2$  signaling pathway mutants, *cost1 atg5-1* and *cost1 atg7-2* double mutants have similar water loss and drought-sensitivity phenotypes to the *atg5-1* or *atg7-2* single mutants, suggesting that autophagy acts downstream of *cost1* in drought tolerance (Fig. 5A–C), and that a functional autophagy pathway is required for drought tolerance in the *cost1* mutant. We also crossed *cost1* with *nbr1*, a mutant defective in the NBR1-selective autophagy adaptor; *nbr1* is unable to recover the *cost1* low water loss phenotype (*SI Appendix*, Fig. S10E), suggesting that *nbr1* is not involved in *cost1*-mediated drought regulation.

As autophagy is also required for tolerance of other stresses, we tested seedling sensitivity to salt. The *cost1* mutant showed a higher survival rate than WT when 150 mM or 200 mM NaCl was included in the growth media (*SI Appendix*, Fig. S12), consistent with a function in autophagy. The role of COST1 in regulating salt and other stress responses warrants further exploration.

***cost1* Mutants Have Increased Basal Autophagy.** To assess autophagosome formation in *cost1* and *cost1 atg* double mutants, osmotic stress was introduced by treating plants with mannitol, a condition known to induce autophagy (30). Roots from plants of various genotypes were stained with MDC (monodansylcadaverine), a fluorescent dye that labels acidic vesicles, primarily autophagosomes, in vivo (57). Upon treatment with mannitol, an increased number of fluorescent puncta were seen in both WT and the *cost1* mutant when compared with control conditions, and as expected this increase was absent in mutants in which *ATG5* or *ATG7* were disrupted (Fig. 5D and E), suggesting that the fluorescent puncta correspond to autophagic structures. Even in the absence of stress, numerous fluorescent puncta were evident in the *cost1* mutant and RNAi lines (*SI Appendix*, Fig. S13), suggesting constitutive activation of the autophagy pathway, and this was completely blocked in *cost1 atg5-1* and *cost1 atg7-2* double mutants (Fig. 5D and E). This indicates that *ATG5* and *ATG7* are required for the potential constitutive autophagy seen in *cost1*, and again positions autophagy downstream of *cost1*.

To confirm the phenotype we observed by MDC staining, *cost1* was crossed with a well-characterized autophagosome marker line, *GFP-ATG8e* (58). Confocal microscopy analysis suggested that the production of GFP-labeled autophagosomes was highly induced under nonstressed conditions in the *cost1* mutant background compared with the WT control (Fig. 6A). Next, we used the release of free GFP to detect autophagic transport and degradation of GFP-ATG8e in the vacuole (58). Immunoblot analysis indicated more free GFP in *cost1/GFP-ATG8e* than in WT/*GFP-ATG8e* both before and after drought treatment (Fig. 6B and *SI Appendix*, Fig. S14), demonstrating that the increase in autophagosome number in the *cost1* mutant is due to increased autophagosome

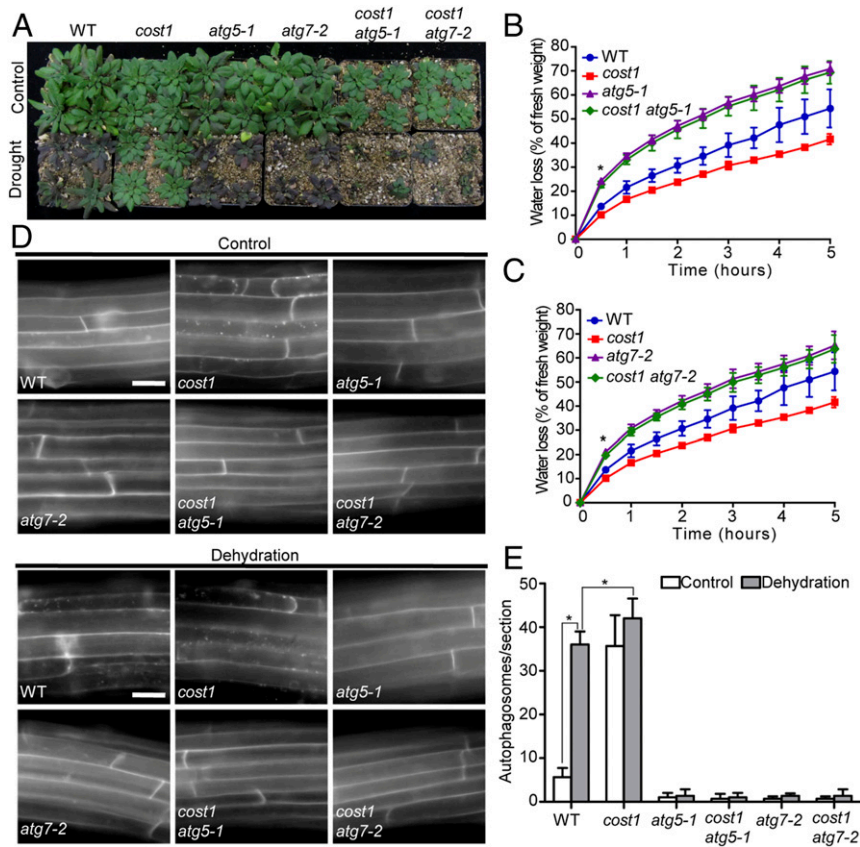


**Fig. 5.** Autophagy is required for drought tolerance of the *cost1* mutant. (A) WT, *cost1*, and the two *cost1 atg* double mutants after exposure to drought for 2 wk. (B and C) Water loss upon drought treatment of *cost1* in combination with *atg5-1* and *atg7-2*. Three independent experiments were done with similar results. Values are means  $\pm$  SE of three replicates and at least 10 leaves from each genotype were assessed per replicate. Asterisks indicate significant difference. (D) Ten-day-old seedlings of the indicated genotypes were treated with or without 300 mM mannitol for 6 h, stained with MDC, and elongation zones of the roots were observed by epifluorescence. (Scale bar, 50  $\mu$ m.) (E) Autophagosomes from D were quantified for at least 10 images per replicate, with 3 biological replicates. Asterisks indicate significant differences.

formation and not decreased degradation. Autophagic flux is therefore higher in the *cost1* mutant than in WT plants.

**Overexpression of *COST1* Leads to *ATG8e* Degradation.** To assess the effect of increased *COST1* protein on autophagy activity, we overexpressed *COST1* in the same GFP-*ATG8e* marker line. RT-PCR (reverse-transcriptase PCR) indicated that the *COST1* gene is highly expressed in all three independent transgenic lines tested (*SI Appendix*, Fig. S15A), and two independent overexpression lines, 35S:*COST1* #35 and #42 were chosen for further study. Note that these lines express much higher levels of *COST1* than the lines used for YFP-*COST1* imaging and localization. First, confocal microscopy was employed to assess the effect of *COST1* overexpression on autophagy. Compared with the GFP-*ATG8e* signal in the absence of *COST1* overexpression, the fluorescence corresponding to GFP-*ATG8e* upon *COST1* overexpression was almost undetectable (Fig. 6A). Next, by immunoblotting using GFP antibodies, we analyzed the cleavage of GFP-*ATG8e* to produce free GFP, as an indicator of flux through the autophagy pathway. A substantial reduction in both full-length GFP-*ATG8e* and free GFP was seen (Fig. 6B and *SI Appendix*, Fig. S16), and this reduction was more evident upon dehydration, consistent with our observations by confocal microscopy (Fig. 6A).

If GFP-*ATG8e* was simply degraded in the vacuole by autophagy upon *COST1* overexpression, we would expect an increase in free GFP in the cleavage assay, which was not observed. To assess whether this effect was specific to the GFP-*ATG8e* transgene-encoded protein, we detected endogenous *ATG8* with

commercially available *ATG8* antibodies, which detect most or all of the *ATG8* isoforms in *Arabidopsis*. The overall *ATG8* protein amount was found to be reduced in the *COST1* overexpression lines (*SI Appendix*, Fig. S17). Meanwhile, compared with WT plants, *COST1* overexpression did not significantly affect the *ATG8e* transcript level, as determined by RT-PCR (*SI Appendix*, Fig. S15A), suggesting that the decrease in *ATG8e* protein occurs posttranscriptionally, possibly due to degradation.

As *ATG8* is a key factor in autophagosome formation, a reduction in the amount of *ATG8* could potentially reduce the capacity of the autophagy pathway. We hypothesized that GFP-*ATG8e* protein might be degraded via the proteasome, thus regulating its availability to function in autophagy. To test this, the *COST1* overexpression plants were treated with the proteasome inhibitor MG132 over a time course of 1 to 4 h. A substantial accumulation of GFP-*ATG8e* was seen after inhibitor treatment (*SI Appendix*, Fig. S15B), indicating that GFP-*ATG8e* is degraded by the proteasome upon *COST1* overexpression. In line with a reduction in autophagy, the *COST1* overexpression transgenic lines are more sensitive to drought and have a higher rate of water loss when compared with WT (Fig. 6C and *SI Appendix*, Fig. S15C).

During an extended length (>60 d) of short-day growth of WT and *cost1*, we observed a delay of leaf senescence and flowering in *cost1* mutant (*SI Appendix*, Fig. S18). Autophagy is strongly associated with nutrient deficiency; to confirm the role of *COST1* in autophagy, we thus assessed the effect of increased and decreased *COST1* on autophagy induction upon carbon and nitrogen starvation. As shown in Fig. 6A, starvation strongly activated autophagy

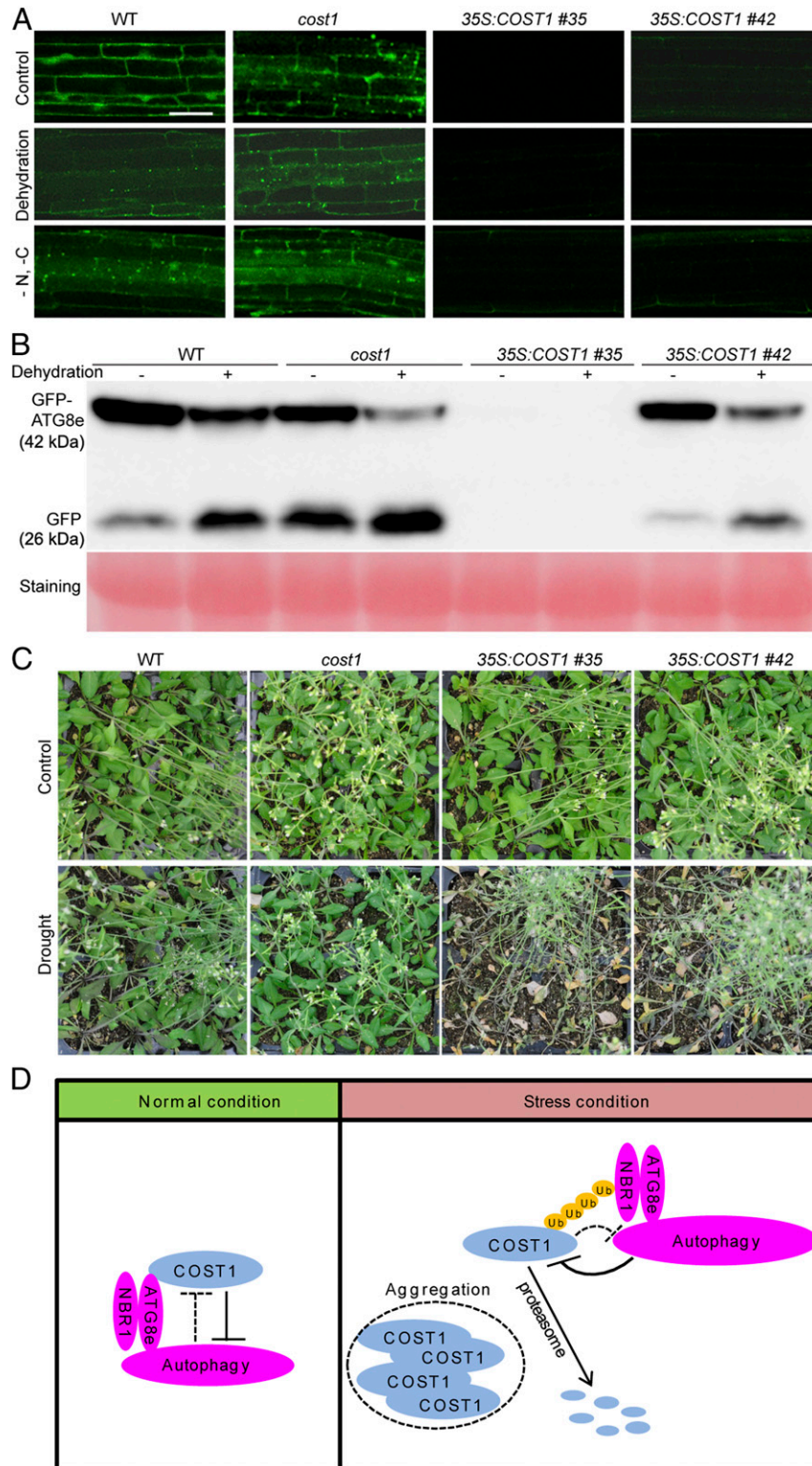


**Fig. 6.** COST1 is a negative regulator of autophagy. (A) Confocal microscopy analysis of autophagy in the same autophagosome marker line GFP-ATG8e in the genetic background of WT, *cost1*, and *COST1* overexpression lines #35 and #42. (Scale bar, 50  $\mu$ m) Ten-day-old seedlings were treated with dehydration for 6 h or starvation for 16 h and representative images are shown. (B) Analysis of GFP-ATG8e cleavage as an indicator of autophagy activity in WT, *cost1*, and two *COST1* overexpression lines with and without 6-h dehydration. Ponceau staining was used as a loading control. (C) Assay for drought tolerance of WT, *cost1*, and two *COST1* overexpression lines. Four-week-old plants of the indicated genotypes were subjected to water withholding for 2 wk and a representative image is shown. (D) A working model of *COST1* function in the drought response. Under normal growth conditions, COST1 inhibits stress responses by directly interacting with ATG8, leading to degradation and thus favoring plant growth. In stress conditions, COST1 proteins are degraded by both the 26S proteasome and autophagy, releasing ATG8, and thus the repression of autophagy, and in turn conferring drought tolerance.

in WT and *cost1*, as evidenced by autophagosome accumulation; but autophagy is substantially reduced when *COST1* is overexpressed. These results indicate that *COST1* negatively regulates autophagy in both drought and starvation conditions. *COST1* is therefore a key factor controlling the tradeoff between growth and stress responses that acts via the regulation of autophagy.

## Discussion

Our phylogenetic analysis showed that *COST* proteins are plant-specific and broadly distributed in all plant species, including mosses. Disruption of the *Arabidopsis COST1* gene caused profound defects in plant growth; the *cost1* mutant is much smaller in size, implying that *COST1* has a pivotal role in growth and cell expansion. The *cost1* mutant also showed a strong drought resistant phenotype, with constitutively higher expression of stress-responsive genes, even under normal conditions, suggesting that *COST1* regulates the balance between growth and stress resistance. *COST1* is annotated as a myosin-4 like protein in the latest update from Araport; however, *COST1* does not show sequence similarity to either of the typical plant myosins, which belong to classes VIII or XI, or to myosin-4 in animals. The basis for the annotation is therefore unclear.

Four closely related *COST* proteins were found in *A. thaliana* but a significant phenotype was observed by disrupting *COST1* alone (Fig. 1 B and D). Meanwhile, only one copy of *COST1* was found in *A. lyrata* and several other plant species analyzed (Fig. 1B). Considering the extremely low transcript level of *COST2*, *COST3*, and *COST4* in our analysis (Fig. 1 B and C), the absolute read count of close to zero for these three genes in the TraVA database (<http://www.travadb.org/>), and the prediction that these genes would not encode full-length proteins, it is likely that these three genes are pseudogenes.

Over the last few decades, key components in plant growth and stress responses have increasingly been found to be regulated by the ubiquitin-proteasome pathway (UPS) (5, 59, 60). Compared with animals, many more protein quality control-related genes are found in the genomes of plant species, including unfolded protein response and proteasome pathway genes (61). For example, ~2,000 E3 ligase and UPS genes are predicted to exist in the genome of *Arabidopsis*, outnumbering those in animals (46). In this study, ubiquitination and the UPS were shown to regulate the abundance of the *COST1* protein (Fig. 3). This suggests that proteins may exist that act as E3 ligases in the degradation of *COST1*, although the identity of these factors remains to be discovered.

In addition to the UPS, autophagy can also efficiently dispose of unwanted proteins, protein aggregates, or organelles (25, 26). In plants, autophagy functions in the response to many stresses, including drought, salt, and oxidative stresses (30, 31). Whereas the ABA and H<sub>2</sub>O<sub>2</sub>-dependent signaling pathways have been widely studied as responsible for drought tolerance, genetic evidence showed that the increased drought resistance of *cost1* is independent of both of these pathways (SI Appendix, Fig. S10 A–D). Instead, our genetic analysis clearly indicates that *atg5-1* and *atg7-2* are epistatic to *cost1* in drought tolerance (Fig. 5), demonstrating that autophagy is required for the *cost1* mutant drought resistance. The *cost1* mutant has constitutively activated autophagy, and *COST1*-YFP interacts with ATG8e and is recruited to autophagosomes upon drought stress. These data suggest that *COST1* both regulates autophagy and is also degraded by the autophagy pathway, a feature shared with the core autophagy regulator ATG1 (62). However, whereas ATG1 is a positive regulator of autophagy, and its degradation results in a balancing feedback loop to allow moderation of the extent of autophagy activation, *COST1* is a negative regulator, and its degradation results in positive feedback, allowing rapid response to stress conditions and therefore promoting plant survival.

Many ATG8-interacting proteins act as selective autophagy adaptors and share a conserved LIR (LC3-interacting region) motif (63). A search for LIR motifs using the online iLIR tool (<http://repeat.biol.ucy.ac.cy/iLIR/>) (64) finds no clear LIR motif in *COST1*, suggesting that *COST1* interacts with ATG8 via a different mechanism. Interestingly, the 26S proteasome core subunit RPN10, which acts as a receptor for selective autophagy of the proteasome, has a distinct motif, termed a UIM (ubiquitin-interacting motif), for recognition by the UIM docking site of ATG8 (65). Narrowing down the specific region of *COST1* that interacts with ATG8 will be an interesting next step in dissecting the underlying mechanism of interaction.

We propose a working model for the function of *COST1* in drought responses (Fig. 6D). Through direct interaction with ATG8, *COST1* inhibits autophagy under normal conditions, thus favoring plant growth. Upon drought stress, *COST1* is ubiquitinated and subjected to degradation by the UPS and autophagy. The subsequent decrease in *COST1* protein levels releases ATG8, allowing autophagosome formation and promoting drought tolerance, while inhibiting growth. TOR (target-of-rapamycin) is a negative regulator of autophagy in plants (66), as in animals and yeast, but many of the upstream regulators of TOR are absent from plants. Plant-specific proteins like *COST1* may provide alternative mechanisms of regulating autophagy and growth in plants. The broad distribution of *COST* genes in land plant species suggest that *COST* family proteins are functionally conserved, raising the possibility of manipulating *COST*-like genes to confer drought tolerance in agricultural species (67).

## Materials and Methods

**Plant Materials and Growth Conditions.** All *A. thaliana* lines used in this study are in the Columbia-0 (Col-0) accession. Five-day-old seedlings grown on half strength MS medium (Sigma-Aldrich) containing 1% (wt/vol) sucrose and 0.8% (wt/vol) agar were transplanted into soil, then kept under 16 h of light and 8 h of dark in a growth chamber at light/22 °C or dark/18 °C. The *cost1-1* T-DNA insertion (*cost1*, SALK\_064001) was confirmed by genomic PCR using the T-DNA left-border primer LBa1 and two *COST1* gene-specific primers (Dataset S1). Disruption of *COST1* gene expression in a homozygous *cost1-1* mutant was confirmed by RT-PCR and qRT-PCR (quantitative RT-PCR). *ACTIN2* was used as an internal control.

Double mutants were obtained by crossing *cost1-1* with *nbr1* (Salk\_135513) (28) and various drought-sensitive mutants, including *abi1-1C* (52), *aba3* (SALK\_054454), *ost1* (SALK\_008068), *ghr1* (SALK\_031493), *atg5-1* (SAIL\_129\_B07) (55), and *atg7-2* (GK-655B06) (56). Genotyping was performed by sequencing for *abi1-1C* and by genomic PCR for the other mutants.

To introduce GFP-ATG8e into the *cost1* mutant background, *cost1* was crossed with a 35S:GFP-ATG8e transgenic line (68). Homozygous plants were confirmed by genomic PCR for *cost1* and kanamycin resistance for GFP-ATG8e.

**Vector Construction and Plant Transformation.** To generate the construct for *cost1* mutant complementation, the genomic DNA sequence including 670 bp upstream of the predicted ATG start codon of *COST1* and 540 bp downstream of the stop codon was amplified by PCR primers *gCOST1F* and *gCOST1R* (Dataset S1), and ligated into the pCAMBIA1300 binary vector after digestion with EcoRI and Sall.

To generate the constructs for *COST1* overexpression, the ORFs were amplified using gene-specific primers (Dataset S1), and inserted into a modified pCAMBIA1300S vector (69) via BamHI and SpeI restriction sites. Two *COST1* overexpression lines used are termed 35S-*COST1*-OX-#35 and -#42.

To construct the vector to knock down the expression of *COST1* by RNAi, a pair of gene-specific primers, *RNAi-COST1F* and *RNAi-COST1R*, were used to amplify a cDNA fragment specific to *COST1* (Dataset S1). The resultant fragment was further introduced into the modified binary vector pFGC5941 (ABRC Stock CD3-447) by a two-step cloning strategy, according to the manufacturer's instructions ([http://www.chromdb.org/rnai/vector\\_info.html](http://www.chromdb.org/rnai/vector_info.html)). The two *COST1* RNAi lines characterized in detail are termed *COST1*-RNAi-#1 and -#3.

To generate the *COST1* promoter-GUS construct, 700 bp upstream of the *COST1* coding region was amplified with *COST1* promoter specific primers *ProCOST1-F* and *PrCOST1-R* (Dataset S1). The 700-bp PCR fragment was digested with BamHI and SmaI and inserted into the pCAMBIA1381Z vector (70). Histochemical analysis by GUS staining was described previously (69).

All constructs were introduced into *Agrobacterium* strain *GV3101* and then into *Arabidopsis* plants by the floral-dip method (42). Transgenic plants were screened on half-MS medium supplemented with 50 mg/L hygromycin and resistant transformants were selected. Transgene expression was assessed in homozygous T<sub>3</sub> progeny.

**Drought Treatment and Water Loss Assay.** To assess drought tolerance, 5-d-old seedlings from different genotypes transplanted to soil were grown for 3 wk. Plants were then subjected to progressive water stress by withholding water for another 2 wk, and images were taken. Equal numbers of plants of different genotypes were grown in the same tray to minimize experimental variation. Measurement of stomatal aperture was based on the ratio of width/length and described in detail previously (71).

To assess water loss, 10 leaves per individual plant of 4-wk-old WT, mutant, complementation, and *RNAi* genotypes were excised, and fresh weights were determined at the designated time intervals. Three replicates were performed. Water loss was represented as the percentage of the initial fresh weight at each time point.

**GST Pull-Down Assay.** For GST-COST1 protein purification, the *COST1* cDNA was inserted into pGEX-4T1 via the EcoR I and Sall sites. After sequence confirmation, the construct was introduced into *Escherichia coli* strain BL21 (DE3). GST-COST1 protein synthesis was induced with 0.3 mM IPTG at 16 °C for 18 h. Purification of GST-COST1 was performed with Glutathione Sepharose 4B beads (GE Healthcare) following the manufacturer's protocol.

To test the interaction between *COST1* and *ATG8e*, the full-length coding sequence of *ATG8e* was subcloned into the pET-28a (+) vector and expressed in BL21 cells to produce a His-*ATG8e* fusion protein. A half-microgram of GST-COST1 or GST alone as control was incubated with glutathione resin (GE) at 4 °C for 1 h with shaking, then 0.5 µg His-*ATG8e* was added. The incubation was continued overnight and the beads were washed several times. The beads were boiled in 2× SDS loading buffer and proteins analyzed by immunoblotting using anti-His (M20001; Abmart) and anti-GST (M20007; Abmart) antibodies.

**BiFC Assay.** BiFC assays were performed in *Nicotiana Benthamiana* leaves, as described previously (69). The firefly LUC enzyme was divided into N-terminal (nLUC) and C-terminal segments (cLUC), and *COST1* and *ATG8e* were separately fused with nLUC and cLUC. The resulting constructs, cLUC-*ATG8e*, *COST1*-nLUC, and vector controls were each introduced into *Agrobacterium* strain *GV3101*. After growth in LB (Luria-Bertani) liquid medium, cells were collected and resuspended in infiltration buffer (10 mM MES, 10 mM MgCl<sub>2</sub>, and 0.15 mM acetosyringone, pH 5.8) to OD<sub>600</sub> = 1.0 (50). Equal volumes of various combinations of *Agrobacterium* strains were mixed and coinfiltrated into *N. benthamiana* abaxial leaves with a needleless syringe. After the infiltration, plants were incubated at 22 °C for 3 d and infiltrated with 1 mM luciferin before observation (50, 72).

**Coimmunoprecipitation.** *Agrobacterium tumefaciens* harboring 35S:GFP and 35S:*COST1*-Flag or 35S:GFP-*ATG8e* and 35S:*COST1*-Flag constructs were coinfiltrated into *N. benthamiana* leaves. Three days after the inoculation, leaves were harvested and quickly frozen in liquid nitrogen. Co-IP buffer (5 mM ethylenediamine tetracetic acid, 100 mM NaCl, 50 mM Tris-HCl, 10% glycerol, 0.2% Nonidet P-40, 0.1% Triton X-100, 50 µM MG132, and complete protease inhibitor mixture tablet, pH 7.5) was used to extract the proteins and the supernatant was centrifuged two times at 18,000 × g for 15 min (50). GFP-Trap beads (10 µL; ChromoTek) were added to 50 mL protein extract and incubated overnight. GFP-Trap beads were then washed three times with co-IP buffer. Bound proteins were released by adding 2× protein loading buffer and boiled for 5 min. For immunoblotting analysis, monoclonal anti-GFP (Sigma-Aldrich) and monoclonal anti-FLAG M2 (Sigma-Aldrich) antibodies were used to detect the relevant fusion proteins (72).

**Confocal Microscopy.** To determine the subcellular localization of *COST1*, 35S:*COST1*-YFP was transiently expressed in *Arabidopsis* protoplasts (73) and analyzed using a confocal microscope at 520-nm and 550-nm wavelengths for excitation and emission (Zeiss LSM 510 META). The empty pA7-YFP vector served as control. Ten-day-old transgenic *COST1*-YFP plants (in *cost1-1* mutant background) were used to characterize the *COST1*-YFP protein localization in response to dehydration. Relative fluorescence intensity was quantified by using imageJ software, the ratios of fluorescence intensity are shown, and signals from YFP alone transgenic plants were set as 1.0.

For colocalization analysis, mCherry was fused to the N terminus of *ATG8e* or *NBR1* in the pAN583 vector. Combinations of equal concentrations of plasmids encoding *COST1*-YFP with mCherry-*ATG8e*, mCherry-*NBR1*, or other

organelle markers were used for cotransformation. Transiently transformed *Arabidopsis* protoplasts were analyzed by confocal microscopy at excitation and emission wavelengths of 520 and 550 nm for YFP, 584 and 607 nm for mRFP, and 575 and 650 nm for mCherry.

**MDC Staining.** MDC staining of mannitol-treated *Arabidopsis* roots was described previously (74). Briefly, 7-d-old seedlings from different genotypes were treated with half MS liquid medium (as the control) or 300 mM mannitol in half MS liquid medium for 6 h, followed by incubation with 0.05 mM MDC for 10 min in the dark. After three brief washes with 1× PBS, samples were observed by epifluorescence microscopy (Carl Zeiss), using a DAPI-specific filter to visualize MDC fluorescence.

**Seed Germination Assay.** The seed germination assay was carried out based on previous studies (69, 70, 75). To minimize experimental variability, *cost1* and WT plants were grown side by side and harvested at the same time. Seeds were sown on the same plate containing MS medium with 2% sucrose and 0.8% agar, supplemented without or with different concentrations of ABA as indicated. Plates were stratified at 4 °C for 3 d and moved to 22 °C with 16-h light and 8-h dark cycles in a growth chamber. Germination greening is defined as the cotyledons that have clearly expanded and turned green. About 100 seeds of *cost1* and WT were used for each experimental treatment, and three biological replicates were performed for statistical analyses.

**Identification of *COST1* Homologs and Their Phylogenetic Analysis.** The amino acid sequences of *COST1* homologs in *A. thaliana* and other plant species were obtained by using the *COST1* protein sequence as query in BLASTp (76) searches against TAIR10 (<https://www.arabidopsis.org>) and Phytozome database v12 (<https://phytozome.jgi.doe.gov/pz/portal.html>) annotated protein sequences, respectively. A match with an E-value ≤ 1e-5 was treated as a potential *COST1* homolog. These potential homologs were then scanned for the presence of the DUF641 domains using the PF04859 hidden Markov model (HMM) from Pfam (77). Sequences with matches above the default threshold were regarded as *COST1* homologs. From the *COST1* homologs, the amino acid sequences of the DUF641 domains were aligned to the HMM using hmmlalign as implemented in HMMER3 (78). The domain sequence alignments were used to infer the *COST1* homolog phylogeny using PhyML v3.0 (79), with the following parameters: -b 500 -m JTT -f e -v e -c 4 -a e. MEGA7.0 (80) was employed for further visualization and editing of the phylogenetic tree. The full-length sequence alignment of protein homologs was created using the Clustalx1.83 program with default settings.

**RNA Extraction and Real-Time PCR.** To analyze transcript levels, qRT-PCR was performed with RNA samples isolated from 10-d-old seedlings grown on half MS media harvested at the indicated times after exposure to 100 µM ABA, 200 mM NaCl, 400 mM mannitol, or drought conditions. Total RNA was extracted with TRIzol reagent (Takara) and treated with RNase-free DNase (Promega). The first strand cDNA was synthesized with the Go Script Reverse Kit (Promega). PCR was performed in 96-well optical reaction plates (CFX Connect) after preincubation for 5 min at 95 °C, followed by 40 cycles of denaturation at 95 °C for 15 s, annealing at 55 °C for 20 s, and extension at 72 °C for 30 s. Amplification of the detected genes was monitored every cycle by SYBR Green fluorescence. All experiments were performed in the CFX Connect real-time PCR detection system using an AceQ qPCR SYBR Green Master Mix (Vazyme Biotech). Results were normalized to the reference gene *ACTIN2* using the ΔΔCt method (81). Each experiment was repeated three times. Primers used in this study are listed in Dataset S1.

**RNA-Seq and Data Analysis.** WT and *cost1* seeds were germinated and seedlings grown vertically on 100-mm × 100-mm square plates (Fisher Scientific) on half-strength MS medium for 10 d. Seedlings were dehydrated for 6 h. Samples were immediately ground and total RNA was extracted using an RNeasy Plant Mini Kit (Qiagen, Cat. No. 74904). RNA-seq libraries were prepared and subjected to paired end sequencing with read length 250 bp. Read counts in each library were normalized using the TMM method, which is the weighted trimmed mean of M-values proposed by Robinson and Oshlack (82), where the weights are from the Δ method on binomial data. Sequences were aligned to the *Arabidopsis* TAIR10 genome, using STAR (v2.4.0). The reads count for each annotated gene were calculated by htseq-count (v0.6.0 with parameters "-t mRNA -m intersection-nonempty-stranded no"; mRNA denotes messenger RNA). Differential gene expression between samples was assessed using negative-binomial generalized-linear models with DESeq2 (83, 84). A gene was considered as expressed in a sample if the average reads per kilobase and million mapped reads (RPKM) among replicates of the gene is >1, and a gene was considered as differentially

expressed between samples if the fold-change between two average RPKM >2. GO functional category information was obtained from TAIR. GO enrichment analysis was conducted using Fisher's exact test, and the *P* values were adjusted to account for multiple testing (85), and the corresponding processed data are listed in [Datasets S2–S4](#).

**Statistical Analysis.** A two-tailed Student *t* test was used for comparison of treatments with the control, and the Fisher's least significant difference test was used for multiple mean comparisons.

**Data Availability.** Raw sequencing data and the processed data for RNA-seq analysis were deposited in the National Center for Biotechnology Gene Expression Omnibus (GEO) under the accession no. GSE113515. Accession numbers for each gene are listed in [Dataset S1](#). Sequence and detailed information

for each gene can be found at TAIR (<https://www.arabidopsis.org/>). All other data are available within the paper and [SI Appendix](#) files.

**ACKNOWLEDGMENTS.** We thank Dr. Liwen Jiang (Chinese University of Hong Kong) for the PVC organelle markers; Mee-Len Chye (University of Hong Kong) for 35S:GFP-ATG8e transgenic plants; and Dr. Kazuo Shinozaki (RIKEN Center for Sustainable Resource Science) for the *abi1-1C* mutant. This work has been jointly supported by the following grants: the National Key R & D Program (2019YFD1000500; 2016YFD0600106); the National Key Program on Transgenic Research (2018ZX08021001); the Modern Agricultural Industry Technology System Innovation Team of Shandong Province of China (SDAIT-02-05); the National Natural Science Foundation of China (31870576); US National Science Foundation (IOS 1353867; to D.C.B.); US National Science Foundation (IOS-1546617 and DEB-1655386); and US Department of Energy Great Lakes Bioenergy Research Center (BER DE-S0018409; to S.-H.S.).

1. E. Pennisi, Plant genetics. The blue revolution, drop by drop, gene by gene. *Science* **320**, 171–173 (2008).
2. R. Mittler, E. Blumwald, Genetic engineering for modern agriculture: Challenges and perspectives. *Annu. Rev. Plant Biol.* **61**, 443–462 (2010).
3. J. K. Zhu, Salt and drought stress signal transduction in plants. *Annu. Rev. Plant Biol.* **53**, 247–273 (2002).
4. K. Yamaguchi-Shinozaki, K. Shinozaki, Transcriptional regulatory networks in cellular responses and tolerance to dehydration and cold stresses. *Annu. Rev. Plant Biol.* **57**, 781–803 (2006).
5. S. Stone, The role of ubiquitin and the 26S proteasome in plant abiotic stress signaling. *Front. Plant Sci.* **5**, 135 (2014).
6. L. Xiong, J. K. Zhu, Regulation of abscisic acid biosynthesis. *Plant Physiol.* **133**, 29–36 (2003).
7. E. Nambara, A. Marion-Poll, Abscisic acid biosynthesis and catabolism. *Annu. Rev. Plant Biol.* **56**, 165–185 (2005).
8. S. Y. Park *et al.*, Abscisic acid inhibits type 2C protein phosphatases via the PYR/PYL family of START proteins. *Science* **324**, 1068–1071 (2009).
9. Y. Ma *et al.*, Regulators of PP2C phosphatase activity function as abscisic acid sensors. *Science* **324**, 1064–1068 (2009).
10. S. R. Cutler, P. L. Rodriguez, R. R. Finkelstein, S. R. Abrams, Abscisic acid: Emergence of a core signaling network. *Annu. Rev. Plant Biol.* **61**, 651–679 (2010).
11. H. Fujii *et al.*, In vitro reconstitution of an abscisic acid signalling pathway. *Nature* **462**, 660–664 (2009).
12. S. C. Lee, W. Lan, B. B. Buchanan, S. Luan, A protein kinase-phosphatase pair interacts with an ion channel to regulate ABA signaling in plant guard cells. *Proc. Natl. Acad. Sci. U.S.A.* **106**, 21419–21424 (2009).
13. G. Pilot *et al.*, Guard cell inward K<sup>+</sup> channel activity in Arabidopsis involves expression of the twin channel subunits KAT1 and KAT2. *J. Biol. Chem.* **276**, 3215–3221 (2001).
14. D. Geiger *et al.*, Activity of guard cell anion channel SLAC1 is controlled by drought-stress signaling kinase-phosphatase pair. *Proc. Natl. Acad. Sci. U.S.A.* **106**, 21425–21430 (2009).
15. J. M. Kwak *et al.*, NADPH oxidase AtrbohD and AtrbohF genes function in ROS-dependent ABA signaling in Arabidopsis. *EMBO J.* **22**, 2623–2633 (2003).
16. Z. M. Pei *et al.*, Calcium channels activated by hydrogen peroxide mediate abscisic acid signalling in guard cells. *Nature* **406**, 731–734 (2000).
17. C. Sirichandra *et al.*, Phosphorylation of the Arabidopsis AtrbohF NADPH oxidase by OST1 protein kinase. *FEBS Lett.* **583**, 2982–2986 (2009). Erratum in: *FEBS Lett.* **583**, 3375 (2009).
18. D. Hua *et al.*, A plasma membrane receptor kinase, GHR1, mediates abscisic acid- and hydrogen peroxide-regulated stomatal movement in Arabidopsis. *Plant Cell* **24**, 2546–2561 (2012).
19. Y. Murata, Z. M. Pei, I. C. Mori, J. Schroeder, Abscisic acid activation of plasma membrane Ca<sup>2+</sup> channels in guard cells requires cytosolic NAD(P)H and is differentially disrupted upstream and downstream of reactive oxygen species production in *abi1-1* and *abi2-1* protein phosphatase 2C mutants. *Plant Cell* **13**, 2513–2523 (2001).
20. R. Antoni, L. Rodriguez, M. Gonzalez-Guzman, G. A. Pizzio, P. L. Rodriguez, News on ABA transport, protein degradation, and ABFs/WRKs in ABA signaling. *Curr. Opin. Plant Biol.* **14**, 547–553 (2011).
21. R. D. Vierstra, The ubiquitin-26S proteasome system at the nexus of plant biology. *Nat. Rev. Mol. Cell Biol.* **10**, 385–397 (2009).
22. F. Yu, Q. Xie, Non-26S proteasome endomembrane trafficking pathways in ABA signaling. *Trends Plant Sci.* **22**, 976–985 (2017).
23. X. Zhuang, Y. Cui, C. Gao, L. Jiang, Endocytic and autophagic pathways crosstalk in plants. *Curr. Opin. Plant Biol.* **28**, 39–47 (2015).
24. R. S. Marshall, R. D. Vierstra, Autophagy: The master of bulk and selective recycling. *Annu. Rev. Plant Biol.* **69**, 173–208 (2018).
25. S. Michaeli, G. Galili, P. Genschik, A. R. Fernie, T. Avin-Wittenberg, Autophagy in plants—What's new on the menu? *Trends Plant Sci.* **21**, 134–144 (2016).
26. Y. Liu, D. C. Bassham, Autophagy: Pathways for self-eating in plant cells. *Annu. Rev. Plant Biol.* **63**, 215–237 (2012).
27. S. Svenning, T. Lamark, K. Krause, T. Johansen, Plant NBR1 is a selective autophagy substrate and a functional hybrid of the mammalian autophagic adapters NBR1 and p62/SQSTM1. *Autophagy* **7**, 993–1010 (2011).
28. J. Zhou *et al.*, NBR1-mediated selective autophagy targets insoluble ubiquitinated protein aggregates in plant stress responses. *PLoS Genet.* **9**, e1003196 (2013).
29. H. Jung *et al.*, Arabidopsis cargo receptor NBR1 mediates selective autophagy of defective proteins. *J. Exp. Bot.* **71**, 73–89 (2020).
30. Y. Liu, Y. Xiong, D. C. Bassham, Autophagy is required for tolerance of drought and salt stress in plants. *Autophagy* **5**, 954–963 (2009).
31. Y. Xiong, A. L. Contento, P. Q. Nguyen, D. C. Bassham, Degradation of oxidized proteins by autophagy during oxidative stress in Arabidopsis. *Plant Physiol.* **143**, 291–299 (2007).
32. L. Chen *et al.*, Autophagy contributes to regulation of the hypoxia response during submergence in Arabidopsis thaliana. *Autophagy* **11**, 2233–2246 (2015).
33. T. Avin-Wittenberg, Autophagy and its role in plant abiotic stress management. *Plant Cell Environ.* **42**, 1045–1053 (2019).
34. S. Signorelli, E. P. Tarkowski, W. Van den Ende, D. C. Bassham, Linking autophagy to abiotic and biotic stress responses. *Trends Plant Sci.* **24**, 413–430 (2019).
35. P. Lamesch *et al.*, The Arabidopsis Information Resource (TAIR): Improved gene annotation and new tools. *Nucleic Acids Res.* **40**, D1202–D1210 (2012).
36. J. Chory *et al.*, National Science Foundation-Sponsored Workshop Report: “The 2010 Project” functional genomics and the virtual plant. A blueprint for understanding how plants are built and how to improve them. *Plant Physiol.* **123**, 423–426 (2000).
37. S. Luhua *et al.*, Linking genes of unknown function with abiotic stress responses by high-throughput phenotype screening. *Physiol. Plant.* **148**, 322–333 (2013).
38. R. D. Finn *et al.*, The Pfam protein families database: Towards a more sustainable future. *Nucleic Acids Res.* **44**, D279–D285 (2016).
39. N. Panchy, M. Lehti-Shiu, S. H. Shiu, Evolution of gene duplication in plants. *Plant Physiol.* **171**, 2294–2316 (2016).
40. R. De Smet *et al.*, Convergent gene loss following gene and genome duplications creates single-copy families in flowering plants. *Proc. Natl. Acad. Sci. U.S.A.* **110**, 2898–2903 (2013).
41. R. Ren *et al.*, Widespread whole genome duplications contribute to genome complexity and species diversity in angiosperms. *Mol. Plant* **11**, 414–428 (2018).
42. S. J. Clough, A. F. Bent, Floral dip: A simplified method for Agrobacterium-mediated transformation of Arabidopsis thaliana. *Plant J.* **16**, 735–743 (1998).
43. H. Yu *et al.*, Activated expression of an Arabidopsis HD-START protein confers drought tolerance with improved root system and reduced stomatal density. *Plant Cell* **20**, 1134–1151 (2008).
44. Z. Y. Wang, L. Xiong, W. Li, J. K. Zhu, J. Zhu, The plant cuticle is required for osmotic stress regulation of abscisic acid biosynthesis and osmotic stress tolerance in Arabidopsis. *Plant Cell* **23**, 1971–1984 (2011).
45. K. Nakashima, K. Yamaguchi-Shinozaki, K. Shinozaki, The transcriptional regulatory network in the drought response and its crosstalk in abiotic stress responses including drought, cold, and heat. *Front. Plant Sci.* **5**, 170 (2014).
46. Z. Hua, R. D. Vierstra, The cullin-RING ubiquitin-protein ligases. *Annu. Rev. Plant Biol.* **62**, 299–334 (2011).
47. B. K. Nelson, X. Cai, A. Nebenführ, A multicolored set of in vivo organelle markers for co-localization studies in Arabidopsis and other plants. *Plant J.* **51**, 1126–1136 (2007).
48. N. Geldner *et al.*, Rapid, combinatorial analysis of membrane compartments in intact plants with a multicolor marker set. *Plant J.* **59**, 169–178 (2009).
49. T. Johansen, T. Lamark, Selective autophagy mediated by autophagic adapter proteins. *Autophagy* **7**, 279–296 (2011).
50. J. Y. Gou, F. F. Felipez, C. J. Liu, D. Weigel, J. W. Wang, Negative regulation of anthocyanin biosynthesis in Arabidopsis by a miR156-targeted SPL transcription factor. *Plant Cell* **23**, 1512–1522 (2011).
51. J. Leung *et al.*, Arabidopsis ABA response gene AB11: Features of a calcium-modulated protein phosphatase. *Science* **264**, 1448–1452 (1994).
52. T. Umezawa *et al.*, Type 2C protein phosphatases directly regulate abscisic acid-activated protein kinases in Arabidopsis. *Proc. Natl. Acad. Sci. U.S.A.* **106**, 17588–17593 (2009).
53. A. C. Mustilli, S. Merlot, A. Vavasseur, F. Fenzi, J. Giraudat, Arabidopsis OST1 protein kinase mediates the regulation of stomatal aperture by abscisic acid and acts upstream of reactive oxygen species production. *Plant Cell* **14**, 3089–3099 (2002).
54. M. Koornneef, K. Leon-Kloosterziel, S. Schwartz, J. Zeevaart, The genetic and molecular dissection of abscisic acid biosynthesis and signal transduction in Arabidopsis. *Plant Physiol. Biochem.* **36**, 83–89 (1998).
55. A. R. Thompson, J. H. Doelling, A. Suttangkakul, R. D. Vierstra, Autophagic nutrient recycling in Arabidopsis directed by the ATG8 and ATG12 conjugation pathways. *Plant Physiol.* **138**, 2097–2110 (2005).
56. T. Chung, A. R. Phillips, R. D. Vierstra, ATG8 lipidation and ATG8-mediated autophagy in Arabidopsis require ATG12 expressed from the differentially controlled ATG12A AND ATG12B loci. *Plant J.* **62**, 483–493 (2010).
57. Y. Pu, D. C. Bassham, Detection of autophagy in plants by fluorescence microscopy. *Methods Mol. Biol.* **1450**, 161–172 (2016).

58. Y. Bao, Y. Mugume, D. C. Bassham, Biochemical methods to monitor autophagic responses in plants. *Methods Enzymol.* **588**, 497–513 (2017).
59. W. J. Lyzenga, S. L. Stone, Abiotic stress tolerance mediated by protein ubiquitination. *J. Exp. Bot.* **63**, 599–616 (2012).
60. D. R. Kelley, M. Estelle, Ubiquitin-mediated control of plant hormone signaling. *Plant Physiol.* **160**, 47–55 (2012).
61. Y. Bao, S. Howell, The unfolded protein response supports plant development and defense as well as responses to abiotic stress. *Front. Plant Sci.* **8**, 344 (2017).
62. A. Suttangkakul, F. Li, T. Chung, R. D. Vierstra, The ATG1/ATG13 protein kinase complex is both a regulator and a target of autophagic recycling in Arabidopsis. *Plant Cell* **23**, 3761–3779 (2011).
63. T. Johansen, T. Lamark, Selective autophagy: ATG8 family proteins, LIR motifs and cargo receptors. *J. Mol. Biol.* **432**, 80–103 (2020).
64. I. Kalvari *et al.*, iLIR: A web resource for prediction of Atg8-family interacting proteins. *Autophagy* **10**, 913–925 (2014).
65. R. S. Marshall, Z. Hua, S. Mali, F. McLoughlin, R. D. Vierstra, ATG8-binding UIM proteins define a new class of autophagy adaptors and receptors. *Cell* **177**, 766–781.e24 (2019).
66. Y. Liu, D. C. Bassham, TOR is a negative regulator of autophagy in Arabidopsis thaliana. *PLoS One* **5**, e11883 (2010).
67. J. I. Schroeder, J. M. Kwak, G. J. Allen, Guard cell abscisic acid signalling and engineering drought hardiness in plants. *Nature* **410**, 327–330 (2001).
68. S. Xiao *et al.*, Overexpression of Arabidopsis acyl-CoA binding protein ACBP3 promotes starvation-induced and age-dependent leaf senescence. *Plant Cell* **22**, 1463–1482 (2010).
69. Y. Bao *et al.*, The tumor necrosis factor receptor-associated factor (TRAF)-like family protein SEVEN IN ABSENTIA 2 (SINA2) promotes drought tolerance in an ABA-dependent manner in Arabidopsis. *New Phytol.* **202**, 174–187 (2014).
70. Y. Bao *et al.*, Characterization of Arabidopsis Tubby-like proteins and redundant function of AtTLP3 and AtTLP9 in plant response to ABA and osmotic stress. *Plant Mol. Biol.* **86**, 471–483 (2014).
71. Y. Zhang *et al.*, SDIR1 is a RING finger E3 ligase that positively regulates stress-responsive abscisic acid signaling in Arabidopsis. *Plant Cell* **19**, 1912–1929 (2007).
72. J. He *et al.*, DEXH box RNA helicase-mediated mitochondrial reactive oxygen species production in Arabidopsis mediates crosstalk between abscisic acid and auxin signaling. *Plant Cell* **24**, 1815–1833 (2012).
73. S. D. Yoo, Y. H. Cho, J. Sheen, Arabidopsis mesophyll protoplasts: A versatile cell system for transient gene expression analysis. *Nat. Protoc.* **2**, 1565–1572 (2007).
74. A. L. Contento, Y. Xiong, D. C. Bassham, Visualization of autophagy in Arabidopsis using the fluorescent dye monodansylcadaverine and a GFP-AtATG8e fusion protein. *Plant J.* **42**, 598–608 (2005).
75. Y. Bao *et al.*, Overexpression of the NDR1/HIN1-like gene NHL6 modifies seed germination in response to abscisic acid and abiotic stresses in Arabidopsis. *PLoS One* **11**, e0148572 (2016).
76. S. F. Altschul *et al.*, Gapped BLAST and PSI-BLAST: A new generation of protein database search programs. *Nucleic Acids Res.* **25**, 3389–3402 (1997).
77. R. D. Finn *et al.*, Pfam: The protein families database. *Nucleic Acids Res.* **42**, D222–D230 (2014).
78. R. D. Finn, J. Clements, S. R. Eddy, HMMER web server: Interactive sequence similarity searching. *Nucleic Acids Res.* **39**, W29–W37 (2011).
79. S. Guindon *et al.*, New algorithms and methods to estimate maximum-likelihood phylogenies: Assessing the performance of PhyML 3.0. *Syst. Biol.* **59**, 307–321 (2010).
80. S. Kumar, G. Stecher, K. Tamura, MEGA7: Molecular Evolutionary Genetics Analysis version 7.0 for bigger datasets. *Mol. Biol. Evol.* **33**, 1870–1874 (2016).
81. Y. Bao, W. M. Song, H. X. Zhang, Role of Arabidopsis NHL family in ABA and stress response. *Plant Signal. Behav.* **11**, e1180493 (2016).
82. M. D. Robinson, A. Oshlack, A scaling normalization method for differential expression analysis of RNA-seq data. *Genome Biol.* **11**, R25 (2010).
83. M. I. Love, W. Huber, S. Anders, Moderated estimation of fold change and dispersion for RNA-seq data with DESeq2. *Genome Biol.* **15**, 550 (2014).
84. Y. Bao *et al.*, IRE1B degrades RNAs encoding proteins that interfere with the induction of autophagy by ER stress in Arabidopsis thaliana. *Autophagy* **14**, 1562–1573 (2018).
85. Y. Benjamini, Y. Hochberg, Controlling the false discovery rate: A practical and powerful approach to multiple testing. *J. R. Stat. Soc. B* **57**, 289–300 (1995).